ON THE TRITRON

G. Hinderer

Physik-Department der Technischen Universität München, D-8046 Garching, W-Germany

Summary

The Tritron is a superconducting separated orbit cyclotron with rather strong longitudinal focusing. The magnetic lattice consists of 12 sectors with alternating gradients. The number ν_s of synchrotron oscillations per turn is comparable to the radial betatron frequency ν_r, which is in contrast to the situation in usual synchrotrons. The coupled radial-longitudinal motion around the central orbit in azimuthally independent fields is described, yielding a combined formula for ν_r and ν_s, which is still valid, if ν_s approaches ν_r. $\nu_s > \nu_r$ turns out to be an unstable situation.

Introduction

At the Munich Accelerator Laboratory the Tritron is under construction, which will be a booster for the existing MP tandem [1,2]. It is a prototype of a separated orbit cyclotron similar to the SOC [3,4], but with magnets and accelerating cavities both superconducting. The Tritron increases the energy of the ions emerging from the tandem by a factor 4-5, thus reaching final energies of e.g. 43 MeV for protons, 21 MeV/u for $^{12}C^{6+}$, or 5.8 MeV/u for $^{127}I^{33+}$.

In fig. 1 a part of the existing accelerator facility and the planned extension is shown. The ion beam is pulsed by a pre-buncher between the ion source and the tandem. It is rebunched after the tandem (PB), yielding short pulses with ~ 0.1 ns duration at the post-stripper PS. The ion pulses are then matched in phase space, injected into the Tritron, and accelerated. The extracted beam is analysed and fed into the existing beam transport system to the experimental area.

The magnet system of the Tritron consists of 12 flat superconducting magnet sectors with 19 resp. 20 neighbouring channel magnets each, guiding the beam on a spiral orbit with a constant turn separation ΔR = 4 cm. A vertical cross section along the radius through a magnet sector is given in fig. 2, showing two adjacent channel magnets. Acceleration is achieved by 6 superconducting cavities providing a maximum voltage gain per turn of 3 MV at extraction. Magnets and cavities hang in a vacuum vessel with an 80 K shield supplying the isolation vacuum as well as the vacuum for the circulating beam. Cross sections of the Tritron are seen in fig. 3, some data are listed in table 1.

The magnetic field of the ~ 240 channel magnets is set individually to guide the central particle of each beam pulse on the central path through the magnets. The mean field on this path is approximatively isochronous. Radial and axial focusing will be achieved by field gradients inside the magnets, alternating from sector to sector. There is also longitudinal focusing, because the mean field for off-momentum particles is not

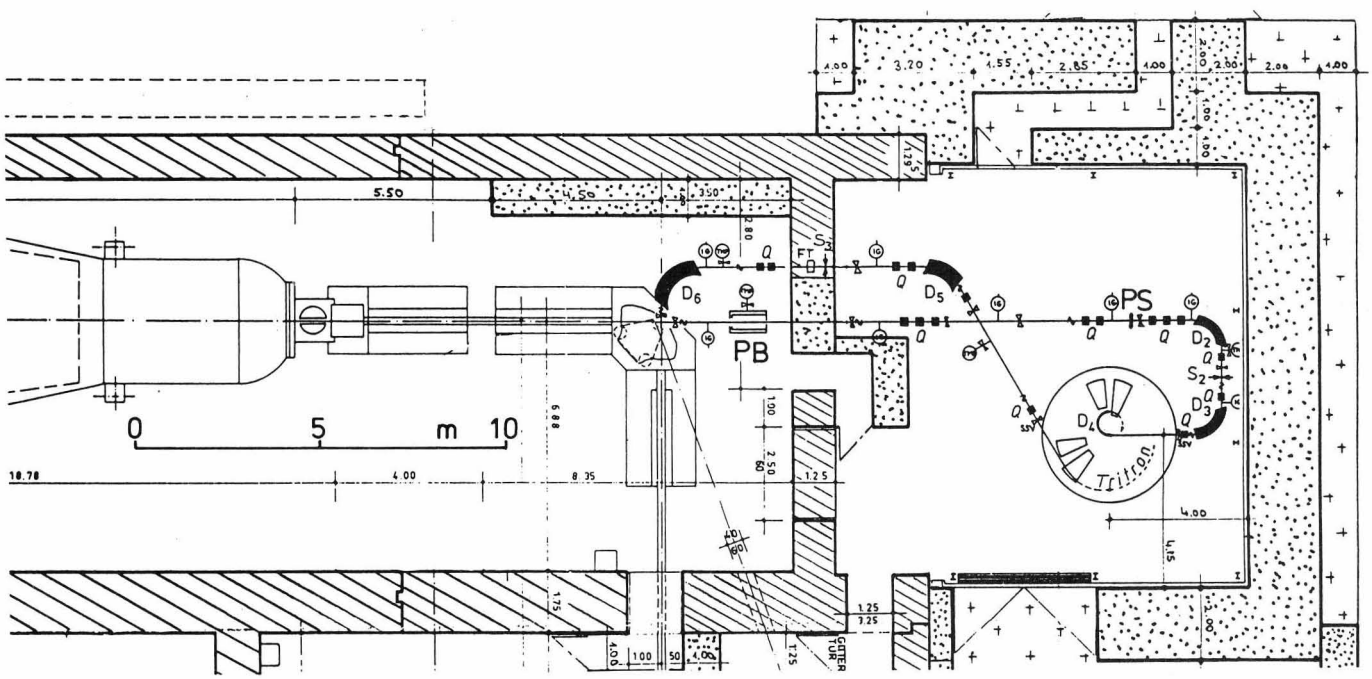

Fig. 1: Plan view of a part of the Munich accelerator facility.
Left side: High energy end of the tandem. Right side: Planned extension with the Tritron.
Bottom: To the existing experimental area. PB: Post-buncher, PS: Post-stripper.

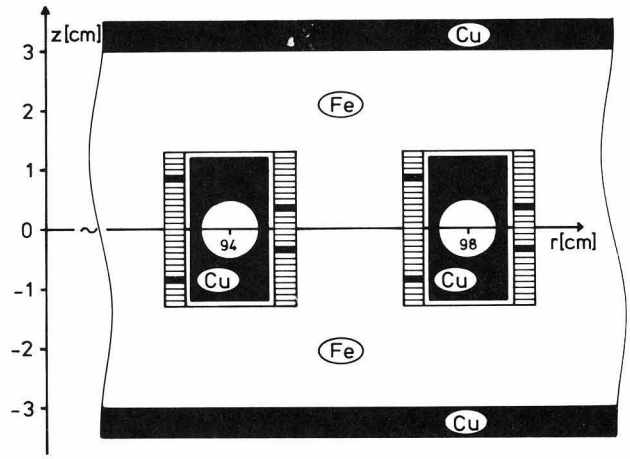

Fig. 2: Vertical cross section through a magnet sector showing two radially adjacent channel magnets.
▭ superconducting cable, Rutherford-type (1.0 x 3.3 mm incl. insulation), 14 strands (Ø 0.4 mm), Cu/NbTi = 1.35, I_{max} = 1320 A
▬ extra turn, made out of the same cable, functioning as gradient layer.
Fe: iron yoke; Cu: radiation shields

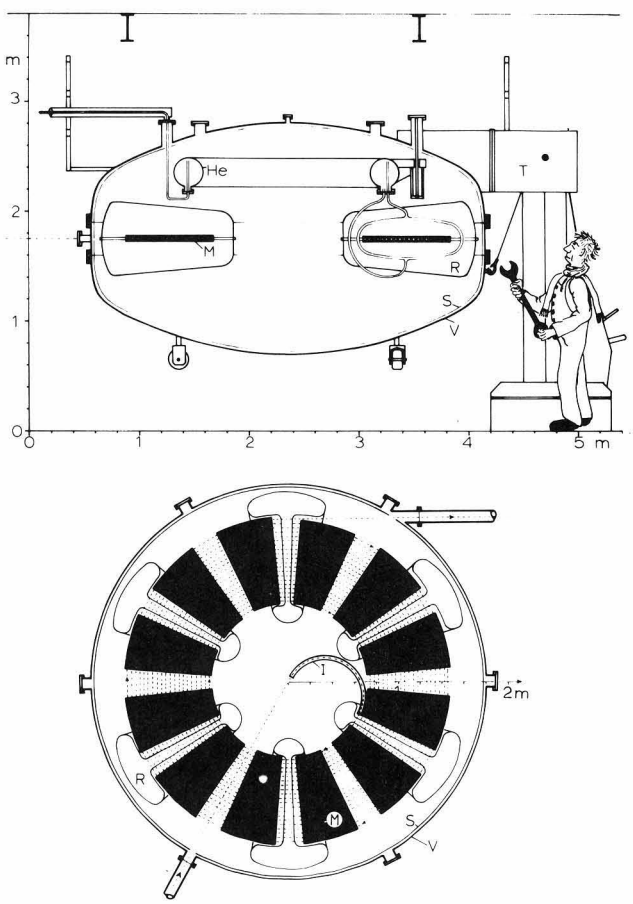

Fig. 3: Cross sections of the Tritron.
M: magnets, R: rf accelerating cavities,
I: injection magnet, V: vacuum vessel,
S: 80 K shield, He: support and liquid helium reservoir, T: support, ion beam: dotted.

isochronous. So the focusing properties of the Tritron are similar to those of a synchrotron. Of course in the Tritron the particles carry out merely 20 turns in individual spiral channels, which requires a large voltage gain per turn. So it resembles in some respects a rolled up linac. Recent investigations about the strong coupling between the radial and the longitudinal particle motion in the Tritron have influenced a design change from weak focusing by means of the entrance- and exit edges of the magnets to strong focusing with alternating gradients. This contribution reports upon these developments.

Table 1: Some Tritron Data

Injector	13 MV tandem
Max. energy: H^{1+} (Q/A = 1)	42.9 MeV
C^{6+} (Q/A = 0.5)	21.3 MeV/u
I^{33+} (Q/A = 0.26)	5.8 MeV/u
Energy gain factor	4.6 - 4.8
Injection radius r(0)	70 cm
Extraction radius r(20)	149 cm
Turn separation ΔR	4 cm
Number of turns	19.7
Number of sectors N	12
Focusing principle	alternating gradients
Number of periodicity N_p	6
Sector angle of a magnet α	20°
Bending field B_{max}	≤ 1.5 T
RF frequency ν_{rf}	160 MHz ± 3%
Harmonic number h	≥ 17
Number of cavities	6
Voltage per cavity U_{max}	500 kV

The central orbit

In an isochronous magnetic field the energy gain per nucleon and turn dT/dm is related to the turn separation dr/dm via

$$\frac{dT}{dm} = m_o \cdot 4\pi^2 f_o^2 r \gamma^3(r) \cdot \frac{dr}{dm} \qquad (1)$$

with m = turn number
$f_o = \nu_{rf}/h$ the constant orbital frequency
h = harmonic number of acceleration
r = mean radius = circumference / 2π
m_o = 931.5 MeV/c^2, $\gamma(r) = (1-\beta^2(r))^{-1/2}$
$\beta(r) = (2\pi r/c) f$, and
$T(r) = (\gamma(r)-1) m_o c^2$

This must be equal to the energy gain achieved by the cavities, which can be written as

$$\frac{dT}{dm} = \frac{Q}{A} \cdot U_o \cdot u(r) \cdot \sin \phi \ (m) \qquad (2)$$

where Q/A means the specific charge of the ions, $U(r) = U_o u(r)$ the peak voltage gain per turn including the transit time factor, u(r) its radial dependence, U_o the voltage set value, and Ø the phase of the particles crossing the center of the cavity with respect to the rf phase. With $r = r_s(m) = r_s(0) + m \cdot \Delta R$ the desired spiral orbit ($r_s(0)$ = 70 cm, ΔR = 4 cm) and U_o high enough (since $|\sin \phi| \leq 1$), the phase curve $\phi_s(m)$ of the central (synchronous) particle can be calculated. There are two solutions for $\phi_s(m)$ because $\sin \phi_s = \sin(\pi - \phi_s)$. For the Tritron with alternating gradients $0 < \phi_s < \pi/2$ is the phase focusing solution.

The phase change $d\phi_s/dm$ can be adjusted[2] by a small deviation from the isochronous magnetic field resulting in a corresponding variation of the central orbital frequency f_s. In fig. 4 T_s, ϕ_s, and $\Delta f_s/f_o = (f_s - f_o)/f_o$ are plotted versus m for Q/A = 0.5 particles, together with the radial dependence u(r(m)) of the accelerating voltage as measured at the prototype cavity. The harmo-

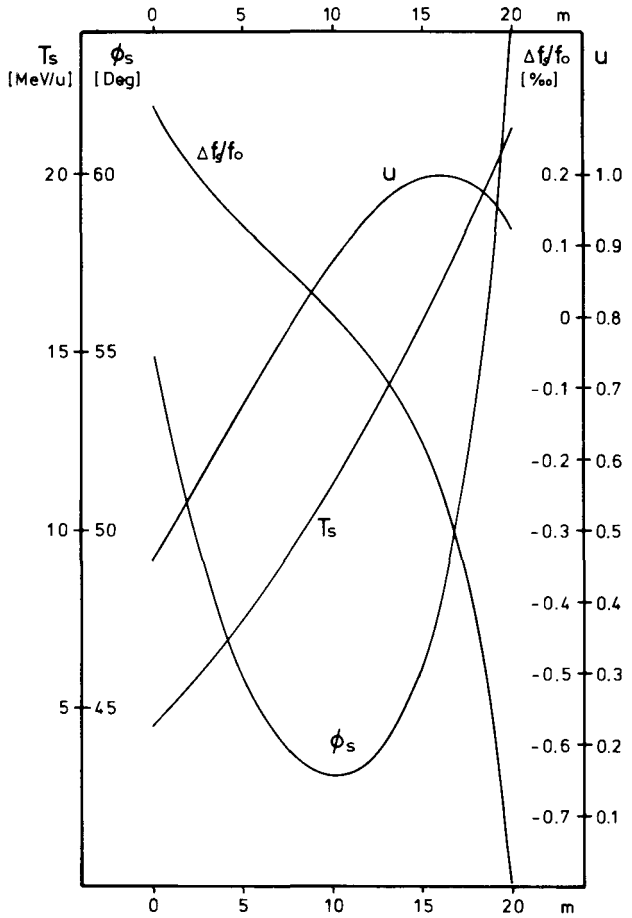

Fig. 4: T_s, ϕ_s and $\Delta f_s/f_o$ as functions of the turn number m for Q/A = 0.5 particles, and the radial dependence u(r) as measured at the prototype cavity, with r(m) = (70 + m · 4) cm, f_o = 6.7 MHz, h = 24, U_o = 2.8 MV.

nic number h = 24 was choosen to meet the measured frequency $\nu_{rf} \approx 160$ MHz of this cavity. The voltage U_o = 2.8 MV leads to sin $\phi_s(20) = 0.90$. The phase curves $\phi_s(m)$ for other ions are similar with a small difference at injection ($\phi_s(0) = 51^o, 55^o, 58^o$ for Q/A = 1, 0.5, 0.26). The frequency deviation $\Delta f_s/f_o$ scales approximately with 1/h.

Synchrotron oscillations

In the last section the accelerated equilibrium orbit for the central particle was described. For particles with momentum deviation $\Delta p/p_s$ there exists a corresponding equilibrium orbit, which is displaced in its mean radius by

$$\Delta r = r_s \cdot \alpha \cdot \frac{\Delta p}{p_s} \tag{3}$$

where α is the momentum compaction factor. The revolution frequency on this orbit differs from f_s by

$$\frac{\Delta f}{f_s} = \frac{\Delta \beta}{\beta_s} - \frac{\Delta r}{r_s} = \left(\frac{1}{\gamma_s^2} - \alpha\right) \cdot \frac{\Delta p}{p_s}$$
$$= \left(\frac{1}{\gamma_s^2} - \frac{1}{\gamma_{tr}^2}\right) \cdot \frac{\Delta p}{p_s} = \eta \cdot \frac{\Delta p}{p_s} \tag{4}$$

γ_{tr} is related to the transition energy T_{tr}. $\eta = 0$ describes the situation in an isochronous field. If $\eta \neq 0$ the frequency deviation causes a phase shift $d\phi/dm$ which in turn results in a different momentum - and energy gain in successive revolutions. Thus - if the synchronous phase ϕ_s is choosen properly, depending on the sign of η - phase - and energy oscillations occur.

These synchrotron oscillations couple to the radial betatron oscillations. Most often the number ν_s of the synchrotron oscillations per turn is much less then the betatron frequency ν_r. Therefore, during one betatron oscillation the momentum of individual particles is nearly constant, and on the average the particles move on their equilibrium orbit defined by eq. (3). Under these circumstances, the radial and longitudinal motion can be treated separately. Provided, the parameters of the central particle do not change too fast, the synchrotron frequency then can be calculated by

$$\nu_s = \sqrt{\frac{\gamma \cdot \eta \cdot h \cdot Q \cdot U \cdot \cos \phi_s}{2\pi(\gamma + 1) \cdot A \cdot T_s}} \tag{5}$$

In the Tritron the voltage $U = U_o \cdot u(r)$ is large to achieve the turn separation. Putting in numbers from the previous design [2] yields $\nu_s \approx 0.15 \ldots 0.60$, and $\nu_r \approx 0.8$. This same order of magnitude for ν_s and ν_r was the reason for looking into the coupled radial - longitudinal motion.

The coupled radial - longitudinal motion

In this section the particle motion in the median plane will be described, neglecting the azimuthal distribution of magnet sectors and cavities. Using polar coordinates the magnetic and electric fields in the median plane may be written

$$B_z = B(r), \quad B_r = B_\varphi = 0 \tag{6}^{*)}$$

$$E_\varphi = -\frac{U(r)}{2\pi r} \cdot \sin(\omega_{rf} t - h \cdot \varphi), \quad E_r = E_z = 0 \tag{7}$$

Choosing the turn number $m = \varphi/2\pi$ as the independent variable, the equations of motion in these fields become

$$p_r' = 2\pi \cdot (p_\varphi - Q \cdot r \cdot B(r)) \tag{8}$$

$$p_\varphi' = -2\pi \cdot \frac{p_r}{p_\varphi} \cdot (p_\varphi - Q \cdot r \cdot B(r)) + \frac{Am_o\gamma}{p_\varphi} \cdot Q \cdot U(r) \cdot \sin \phi \tag{9}$$

$$r' = 2\pi r \cdot \frac{p_r}{p_\varphi} \tag{10}$$

$$\phi' = -2\pi h \cdot \frac{f - f_o}{f} \tag{11}$$

where the prime denotes the derivative d/dm.

$$\phi = \omega_{rf} t - h \cdot \varphi \tag{12}$$

is the phase of the particle with respect to the rf - phase,

$$f = \frac{dm}{dt} = \frac{p_\varphi}{Am_o\gamma} \cdot \frac{1}{2\pi r} \tag{13}$$

is the momentary revolution frequency, and

$$f_o = \frac{\omega_{rf}}{2\pi h} \tag{14}$$

The magnetic field B(r) shall be adjusted for the synchronous particle moving on the desired spiral orbit $r_s(m)$, yielding the phase curve $\phi_s(m)$, the momenta

*) B(r) shall include the magnetic rf-field, rising from a radial change of the electric field.

$p_{rs}(m)$, $p_{\varphi s}(m)$, and the energy $T_s(m)$. For particles with small deviations Δr, $\Delta\phi$, Δp_r, and Δp_φ the equations of motion in these coordinates are achieved by subtracting the central orbit motion. Retaining only linear terms, and with the turn separation $r_s' = \Delta R \ll r_s$, results in

$$\Delta p_r' = 2\pi \cdot p_s \cdot \left[\frac{\Delta p_\varphi}{p_s} - (1 - n) \cdot \frac{\Delta r}{r_s} \right] \tag{15}$$

$$\Delta p_\varphi' = p_s \cdot \frac{\Delta R}{r_s} \cdot \left[\gamma^2 \cdot \cot g\ \phi_s \cdot \Delta\phi - 2\frac{\Delta p_\varphi}{p_s} + (1 - n - \gamma^2 \cdot n_e) \cdot \frac{\Delta r}{r_s}\right] \tag{16}$$

$$\Delta r' = 2\pi \cdot r_s \cdot \frac{\Delta p_r}{p_s} \tag{17}$$

$$\Delta\phi' = -2\pi h \cdot \left[\frac{1}{\gamma^2} \cdot \frac{\Delta p_\varphi}{p_s} - \frac{\Delta r}{r_s}\right] \tag{18}$$

where

$$n = -\frac{r_s}{B(r_s)} \cdot \frac{dB}{dr}\Big|_{r_s} \quad \text{and} \quad n_e = -\frac{r_s}{U(r_s)} \cdot \frac{dU}{dr}\Big|_{r_s} \tag{19}$$

are the magnetic and the electric field indices. These four linear differential equations of first order describe the coupled radial - longitudinal motion with small amplitudes around the central orbit. The motion can be decoupled by further differentiation, yielding one differential equation of fourth order for each separated coordinate. Regarding the expressions ΔR, γ, and r_s/p_s as constants, this procedure leads to the following equation for the radial deviation $\Delta r(m)$:

$$\Delta r'''' + \alpha_3 \cdot \Delta r''' + \alpha_2 \cdot \Delta r'' + \alpha_1 \cdot \Delta r' + \alpha_o \cdot \Delta r = 0 \tag{20}$$

with the coefficients

$$\alpha_o = -4\pi^2 \cdot \{\cot g\ \phi_s \cdot [2\pi h \cdot \frac{\Delta R}{r_s} \cdot (n - 1 + \gamma^2) - \gamma^2 \cdot \phi_s''] + \frac{(tg\ \phi_s)'}{tg\ \phi_s} \cdot [\frac{\Delta R}{r_s} \cdot (n - 1 + \gamma^2 \cdot \sin^2\ \phi_s) + n'] + n'' + 2\frac{\Delta R}{r_s} \cdot n'\} \tag{21}$$

$$\alpha_1 = -4\pi^2 \cdot \{\frac{(tg\ \phi_s)'}{tg\ \phi_s} \cdot (n - 1 - \gamma^2 \cdot \cos^2\ \phi_s) + \frac{\Delta R}{r_s} \cdot (2n - 2 + \gamma^2) + 2n'\} \tag{22}$$

$$\alpha_2 = 4\pi^2 \cdot (1 - n) + \frac{\Delta R}{r_s} \cdot [2\pi h \cdot \cot g\ \phi_s + 2 \cdot \frac{(tg\ \phi_s)'}{tg\ \phi_s}] \tag{23}$$

$$\alpha_3 = 3 \cdot \frac{\Delta R}{r_s} + \frac{(tg\ \phi_s)'}{tg\ \phi_s} \tag{24}$$

If ϕ_s does not change too fast, the most dominant coefficients are α_o and α_2. Assuming

$$\alpha_o = \text{const}, \quad \alpha_2 = \text{const}, \quad \alpha_1 = \alpha_3 = 0 \tag{25}$$

leads to the solution

$$\Delta r(m) = A_1 \cdot \cos(\omega_1 m + \beta_1) + A_2 \cdot \cos(\omega_2 m + \beta_2) \tag{26}$$

with

$$\omega_{1/2} = [\frac{\alpha_2}{2} \pm \sqrt{\frac{\alpha_2^2}{4} - \alpha_o}]^{1/2} \tag{27}$$

Both frequencies are real, and the oscillation is stable, if

$$0 < \alpha_o < \frac{\alpha_2^2}{4} \text{ and } \alpha_2 > 0 \tag{28}$$

ω_1 and ω_2 are the betatron - and the synchrotron frequencies

$$\nu_r = \omega_1/2\pi, \quad \nu_s = \omega_2/2\pi \tag{29}$$

Neglecting the derivatives of ϕ_s and n, α_o and α_2 may be written as

$$\alpha_o \approx -8\pi^3 \cdot a \cdot (\gamma^2 - 1 + n) \tag{21a}$$

$$\alpha_2 = 4\pi^2 \cdot (1 - n) + 2\pi a \tag{23a}$$

with

$$a = h \cdot \frac{\Delta R}{r_s} \cdot \cot g\ \phi_s = \frac{h \cdot Q \cdot U \cdot \cos\ \phi_s}{\gamma \cdot (\gamma + 1) \cdot A \cdot T_s} \tag{30}$$

In the last expression the relation between the turn separation and the energy gain in an isochronous field has been used. If

$$\alpha_o \ll \frac{\alpha_2^2}{4} \tag{31}$$

equation (27) simplifies to

$$\omega_1 = \sqrt{\alpha_2}, \quad \omega_2 = \sqrt{\alpha_o/\alpha_2} \tag{27a}$$

resulting in $\nu_s \ll \nu_r$. With the additional assumption

$$|a| \ll 2\pi \cdot |1 - n| \tag{32}$$

ν_r becomes

$$\nu_r = \sqrt{1 - n} \tag{33}$$

the well known formula for the radial betatron frequency in an azimuthally constant magnetic field, and ν_s results in

$$\nu_s = \sqrt{a \cdot \gamma^2 \cdot \eta/(2\pi)} = \sqrt{\frac{\gamma \cdot \eta \cdot h \cdot Q \cdot U \cdot \cos\ \phi_s}{2\pi(\gamma + 1) \cdot A \cdot T_s}} \tag{34}$$

with

$$\eta = (\frac{1}{\gamma^2} - \frac{1}{1-n}) = (\frac{1}{\gamma^2} - \frac{1}{\gamma_{tr}^2})$$

which is the synchrotron formula eq. (5). The momentum compaction factor becomes under these conditions $\alpha = 1/(1 - n)$.

In the Tritron $|a|$ is rather high especially for the slowly moving heavy ions, reaching at injection with $\Delta R = 4$ cm, $r_s = 70$ cm, $\phi_s \approx 55^o$, and $h \approx 50$ the value $|a| \approx 2$. In fig. 5 ν_r and ν_s are plotted versus n for $|a| = 1.9$ and $T_s = 4.5$ MeV/u according to the formula (27) (solid lines), and for comparison also with the equations (33) and (34) (broken lines). At $n_{tr} = 1 - \gamma^2 = -0.01$ ν_s vanishes. For $n > n_{tr}$ a has to be choosen negative, so $\pi/2 < \phi_s < \pi$ (above transition). For $n < n_{tr}$ the stable motion requires $a > 0$, $0 < \phi_s < \pi/2$ (below transition). At $n_g = 0.2\ \alpha_o$ becomes equal to $\alpha_2^2/4$, resulting in $\nu_r = \nu_s$. Beyond this point

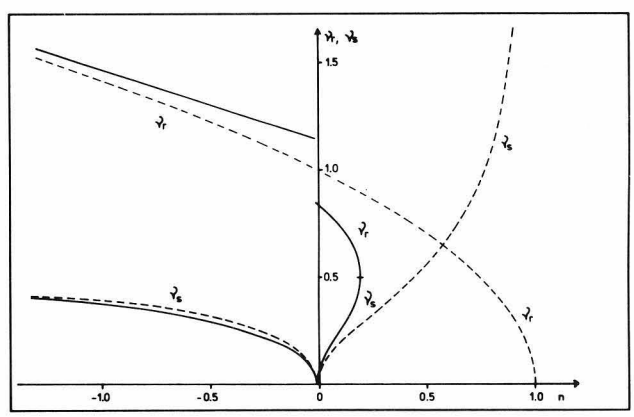

Fig. 5: ν_r and ν_s versus field index n. Solid curves according to eq. (27), broken lines with the approximated formulas eq. (33) and (34) $|a| = 1.9$, $T_s = 4.5$ MeV/u.

for values $n > n_g$ the motion contains two oscillations with the same frequencies, one with an exponentially increasing, the other with decreasing amplitude.

In the previous weak focusing design[2] the effective field index has been choosen to be n = 0.4. Due to the strong coupling between the radial and the longitudinal motion this is an unstable situation at least for heavy ions near injection. Going to negative values for n requires alternating gradients for retaining stability of the vertical motion. The magnetic lattice described in the next section leads to an effective field index,which varies almost linearly with the turn number m, with $n(0) \approx -0.75$ and $n(20) \approx -1.60$. With this choice the conditions of eq. (31) and (32) are valid, and the usual formulae for the betatron - and synchrotron frequencies may be used.

The influence of the terms α_1 and α_3 and the variation of α_0 and α_2 with m on the radial motion can be regarded as a perturbation of the solution $\Delta r(m)$ given in equation (26). For the Tritron it turns out that this contribution is negligible, reflecting the fact that the change of the central orbit parameters is still adiabatic. This agrees with the condition for the adiabaticity parameter[5] $\varepsilon \ll 1$, since the maximum value for ε is ~ 0.15 (for protons at extraction).

For the coupled radial - longitudinal motion in azimuthally constant fields also the four - dimensional eigenellipsoid has been calculated[6], giving e.g. the matching conditions at injection. Projections of this ellipsoid on two planes show tilted ellipses, describing the correlation between the longitudinal momentum deviation $\Delta p_\varphi/p_s$ and the radial position Δr (dispersion or momentum compaction) and the correlation between the radial angle $\Delta\theta = \Delta p_r/p_s$ and the longitudinal phase $\Delta\varphi$ (resulting in constant center position phase). Both correlations can be introduced by a dispersion matching system, but not independently from each other. As a consequence fully matching on the eigenellipsoid is only possible, if the uncoupled horizontal and longitudinal subspaces (e.g. at the post stripper position in fig. 1) have the same area (i.e. $\Delta x \cdot \Delta p_x = \Delta t \cdot \Delta T$). In table 2 the envelopes of the eigenellipsoid at injection and extraction are listed, together with some other data. The momentum compaction factor α is the dispersion of the eigenellipsoid divided by the radius r_s. It is somewhat smaller than $1/(1-n)$ due to the radial - longitudinal coupling. Generally the longitudinal focusing modifies the momentum compaction factor according to $1/\alpha$ (with rf) = $1/\alpha$ (without rf) $\pm \nu_s \cdot \nu_r$, with the plus sign for $\gamma < \gamma_{tr}$ and minus for $\gamma > \gamma_{tr}$. The data for the envelopes may be regarded as average values along one orbit for the beam pulses traveling through the discrete magnetic lattice described in the next chapter.

Table 2: Some data for light, medium heavy, and heavy ion beams (e.g. protons, $^{12}C^{6+}$, and $^{127}I^{33+}$). For each Q/A value the left column corresponds to injection, the right column to extraction. The phase space is assumed to be the four - dimensional eigenellipsoid with the radial emittance at injection $\varepsilon_r = \pi \cdot \Delta r_o \cdot \Delta\theta = 2\pi$ mm mrad. Here Δr_o is the half radial width without the contribution from the energy-spread ($\approx$ 10 % smaller than Δr) α is the momentum compaction factor. The field index is n = - 0.75 at injection and n = - 1.60 at extraction.

	Q/A = 1		Q/A = 0.5		Q/A = 0.26	
T_s (MeV/u)	8.9	42.9	4.5	21.3	1.3	5.8
φ_s (Deg)	51.3	64.2	54.9	64.2	57.5	64.2
f_o (MHz)	9.34		6.69		3.53	
h	17		24		46	
ν_r	1.35	1.62	1.36	1.62	1.38	1.63
ν_s	0.22	0.14	0.25	0.17	0.32	0.24
$\pm\Delta r$ (mm)	1.12	0.94	1.13	0.95	1.15	0.96
$\pm\Delta\theta$ (mrad)	1.93	0.99	1.93	0.99	1.92	1.00
$\pm\Delta t$ (ps)	42	26	56	35	95	58
$\pm\Delta T/T_s$ (‰)	2.49	0.79	2.61	0.85	2.97	0.99
α	0.49	0.35	0.48	0.35	0.46	0.33

The magnetic lattice

In the present design each of the 12 magnet sectors has an azimuthal width of 20°. The entrance and exit faces of each channel have been choosen rectangular to the central orbit, making the end pieces of the channel magnets easier to fabricate. Since the bending angle of each magnet is 360°/12 = 30° this leads to a sawtooth - like field boundary for radially adjacent channels with zero focusing angles at the entrance and exit. Inside the magnets there will be a field gradient having the same sign for all magnets of one sector, but alternating from sector to sector.

The superconducting coil of each half-magnet[1] consists of 12 turns of a Rutherford-type cable (dimensions 1.0 x 3.3 mm including insulation), carrying a current $I \leq 1320$ A. There is one additional turn made from an extra piece of the same cable which is put between turn number 3 and 4 on one side and between turn number 8 and 9 on the other side of the channel (see fig. 2). This gradient layer may carry a current different from the main current or simply function as an insulation layer. With the code POISSON magnetic field calculations have been performed[7] showing the most linear change of the field if the center of the right and left side layer is positioned at 26% and 63% of the half-gap height respectively. For the 1 mm thick insulation layer the magnetic field versus radius is shown in fig. 6. The gradient, divided by the field at the center of the magnet is - 3.6/m, changing the sign, if the height positions of the layer are interchanged. With the bending radius of the magnets beeing $\sim 2/3 \cdot 0.7$ m at injection and $\sim 2/3 \cdot 1.5$ m at extraction this alternating gradient leads to a linear increase from n = ± 1.65 to n = ± 3.54 between turn number 0 and 20.

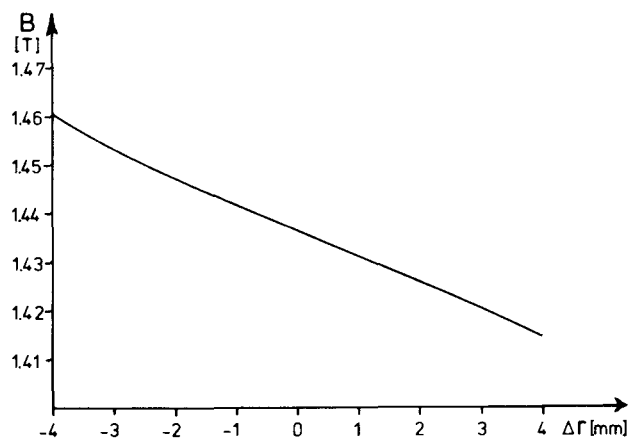

Fig. 6: Magnetic field inside one magnet channel versus the radius deviation for the cross section shown in fig. 3. $\Delta r = 0$ is the center of the channel. Zero current in the gradient layer.

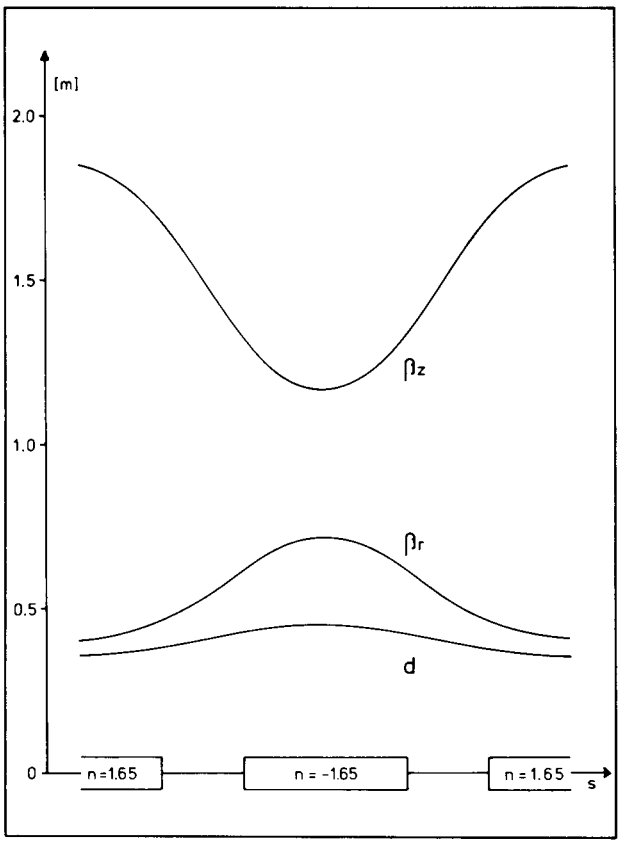

Fig. 7: The radial- and axial ß-functions on the path s through one cell of the magnetic lattice at injection, together with the dispersion d (for $\Delta p/p = 1$).

In fig. 7 the radial- and axial ß-functions at injection are shown for one of the six cells of a closed orbit (no acceleration), together with the dispersive function d for $\Delta p_\varphi/p_s = 1$. In table 3 some data at the center position of the two magnets of a cell are presented for injection and extraction. The radial - and axial beam envelopes Δr and Δz result from $\sqrt{\varepsilon \cdot \beta/\pi}$, with $\varepsilon = 2\pi$ mm mrad the emittance at injection and $(2 \cdot 0.7/1.5)\ \pi$ mm mrad at extraction. The momentum compaction α is the mean value of the dispersion d, divided by the mean radius. Equating $1/\alpha = \gamma_{tr}^2 = (1 - n_{eff})$ leads to the values $n_{eff} = -0.75$ and - 1.60 used in the calculations for table 2. The value for ν_r at extraction is larger in table 3 than in table 2, because $\nu_r > \sqrt{1 - n_{eff}}$ in alternating gradient machines, with increasing deviation for larger alternating field indices.

Table 3: Closed orbit data without acceleration for the magnetic lattice with zero current in the gradient layers. The data correspond to the center of the magnets with field index n. The assumed radial and axial emittances are 2π mm mrad at injection and - inversely to the radius increase - $(2 \cdot 0.7/1.5)\ \pi$ mm mrad at extraction.

	Injection		Extraction	
n	1.65	-1.65	3.54	-3.54
β_r (m)	0.41	0.72	0.47	1.91
β_z (m)	1.85	1.16	2.53	0.86
d (m)	0.36	0.45	0.43	0.73
± Δr (mm)	0.90	1.20	0.66	1.33
± Δθ (mrad)	2.22	1.67	1.41	0.70
± Δz (mm)	1.92	1.53	1.54	0.90
± Δφ (mrad)	1.04	1.31	0.61	1.04
α	0.57		0.38	
ν_r	1.34		1.74	
ν_z	0.49		1.09	

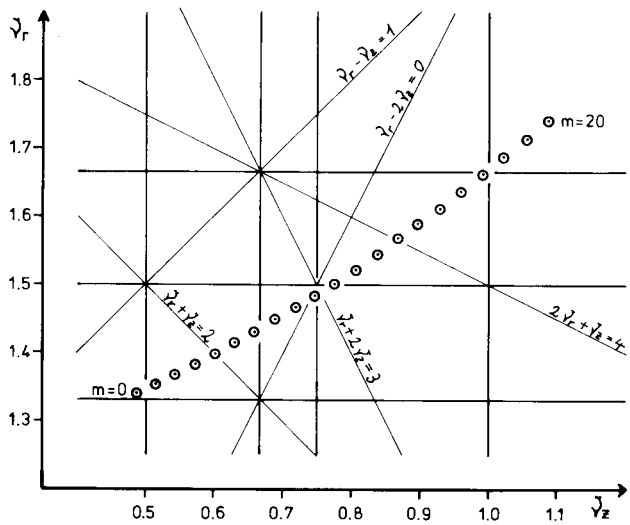

Fig. 8: Resonance diagramm $\nu_r - \nu_z$, with some lower order resonance lines. The dots correspond to the turns m = 0 to m = 20. Zero current in the gradient layers of the magnets.

In fig. 8 ν_r is plotted versus ν_z for the 20 turns between injection and extraction. The data correspond to zero current in the gradient layers. A current with the same direction in the positive and negative gradient layer would shift the (ν_r, ν_z)- values along the curve. Coupled inversely a gradient current results in a parallel displacement of the $\nu_r - \nu_z$ curve.

There are some resonant lines to be crossed between injection and extraction. For a perfect machine this probably would not harm at all, since they are crossed rather fast. The magnetic field inside the channels however contains higher multipole components. So the Taylor series up to fourth order for the field curve shown in fig. 6 is given by $B(\Delta r) = B(0) \cdot (1 - 3.6 \cdot 10^{-3} \cdot \Delta r/\text{mm} - 24 \cdot 10^{-6} \cdot (\Delta r/\text{mm})^3 + 2.8 \cdot 10^{-6} \cdot (\Delta r/\text{mm})^4)$. The heights of the gradient layers have been optimised for a vanishing quadratic term. In order to find tolerance limits for these field perturbations calculations have been performed with the code TURTLE[8] using different third, fourth, and especially second order contributions in the bending fields. As a result the beam acceptance decreases with increasing quadratic term. Inside a certain area the beam is nearly unaffected, outside the particles are lost after a few turns. For an axial- and radial emittance of 10 π mm mrad the tolerance limit of the second order term is about $100 \cdot 10^{-6}$ mm^{-2}. This is the value of the curve in fig. 6, if the Tayler series is centered at $\Delta r \approx -1$ mm. Calculations with different field gradients moving along the tune line of

fig 8 do not indicate a significant change in the toterance limit when approaching or crossing a resonance. More detailed investigations about these questions are on the way.

This work has been inspirited by many discussions with members of the Tritron group. Especially I wish to return thanks to my collegues Uwe Trinks and Cornelius Riess, who has performed a lot of calculations about the beam dynamics.

Work supported by the Federal Government of Germany, Minister for Research and Technology.

References

1. U. Trinks, W. Assmann, G. Hinderer, Nucl. Instr. and Meth. A244 (1986) 273.
2. G. Hinderer, U. Trinks, Nucl. Instr. and Meth. A244 (1986) 283.
3. F.M. Russel, Nucl. Instr. and Meth. 23 (1963) 229.
4. J.A. Martin, IEEE Trans. Nucl. Sci NS-13(1966)288.
5. B.W. Montague, CERN 77-13 (1977) p. 68.
6. G. Hinderer, Internal report, TUM, August 1986 (in German).
7. R. Savoy, Internal report, TUM, Februar 1986 (in German).
8. D.C. Carey, NAL-64 (1971).